ACS APPLIED MATERIALS & INTERFACES

Research Article

www.acsami.org

Conversion of Nanocellulose Aerogel into TiO_2 and TiO_2@C Nanothorns by Direct Anhydrous Mineralization with $TiCl_4$. Evaluation of Electrochemical Properties in Li Batteries

Aurélien Henry,[†,‡,⊥] Sandrine Plumejeau,[†] Laurent Heux,[§] Nicolas Louvain,[‡,⊥] Laure Monconduit,[‡,⊥] Lorenzo Stievano,[‡,⊥] and Bruno Boury*[,†]

[†]Institut Charles Gerhardt Montpellier UMR 5253 - CMOS Pl. E. BATAILLON 34090 Montpellier, France

[‡]ICG-AIME, Université Montpellier 2, Bat. 15, cc 15-02, Pl. E. Bataillon, 34095 Montpellier Cedex, France

[⊥]Réseau sur le Stockage Electrochimique de l'Energie (RS2E), CNRS FR3459, 33 Rue Saint Leu, 80039 Amiens Cedex, France

[§]Centre de Recherches sur les Macromolécules Végétales (CERMAV-CNRS), BP 53,F-38041 Grenoble Cedex 9, France

Supporting Information

ABSTRACT: Nanostructured TiO_2 and TiO_2@C nanocomposites were prepared by an original process combining biotemplating and mineralization of aerogels of nanofibrillated cellulose (NFC). A direct one step treatment of NFC with $TiCl_4$ in strictly anhydrous conditions allows TiO_2 formation at the outermost part of the nanofibrils while preserving their shape and size. Such TiO_2@cellulose composites can be transformed into TiO_2 nanotubes (TiO_2-NT) by calcination in air at 600 and 900 °C, or into TiO_2@C nanocomposites by pyrolysis in argon at 600 and 900 °C. Detailed characterization of these materials is reported here, along with an assessment of their performance as negative electrode materials for Li-ion batteries

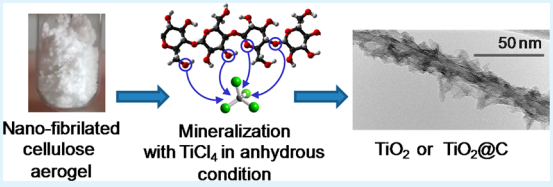

KEYWORDS: *nanocelullose, titanium dioxide, mineralization, TiO_2/C composite, electrochemistry*

INTRODUCTION

Metal oxides such as TiO_2 are materials in high demand for new technologies. Their properties can be finely tailored by varying the porosity, crystallinity, morphology, doping, particle size, and, last-but-not-least, their arrangement in hierarchical macro-, nano-, and microscale structures. With increased emphasis on "green" chemistry, interest in sustainable processes is aimed at minimizing the use of toxic chemicals, solvents, energy, etc. Accordingly, inorganic replication of biotemplates with polysaccharides (cellulose, chitosan and chitin, agarose, starch, carrageenan, etc.) has been actively explored in the field of metal oxide synthesis.[1,2]

We recently reported a completely new approach whereby cellulosic fibers are considered as a template and also as a reagent from which oxygen atoms are transferred to a metal atom of a metal chloride (Figure 1).[3,4] This direct one-step process is a type of mineralization that avoids preparation of any metal oxide sol or the use of sophisticated ALD equipment. Moreover, it allows the formation of TiO_2 with unusual morphological features, such as urchins and carpets of needles, which has never been noted with other processes. It is a solid/liquid process, and it is noteworthy that the phenomena occurring at the interface of the cellulose fibers are essential for maintaining the characteristic of the material. In this sense, increasing the surface accessible to the reaction is likely to enhance the properties of such materials.

In this sense, nanocelluloses, such as bacterial cellulose (BC), cellulose nanocrystals (CNC), microfibrillated cellulose

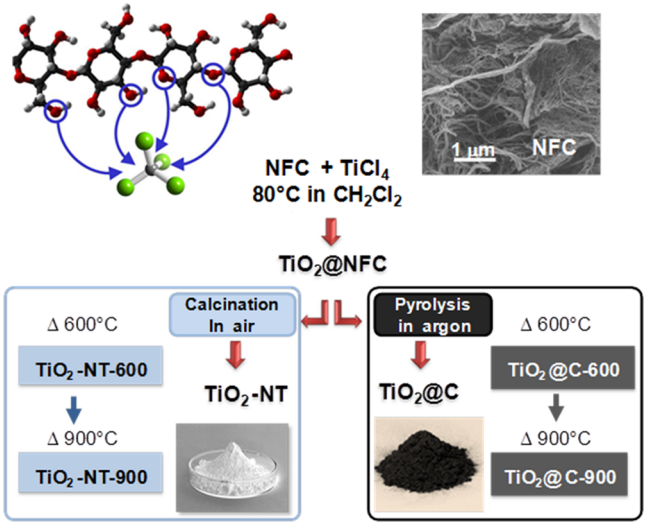

Figure 1. General overview of the process, nomenclature, and preparation of TiO_2-NT and TiO_2@C samples by thermal treatment of the initial TiO_2@NFC nanocomposite obtained by $TiCl_4$ treatment of NFC materials.

Received: January 15, 2015
Accepted: April 16, 2015
Published: April 16, 2015

ACS Publications © 2015 American Chemical Society

DOI: 10.1021/acsami.5b00299
ACS Appl. Mater. Interfaces 2015, 7, 14584−14592

(MFC), and nanofibrillated cellulose (NFC), are sustainable, abundant, inexpensive, and environmentally friendly nanomaterials that exhibit interesting properties due to their nanometric scale.[5,6] They have been considered for uses in nanocomposites, as well as in medical and life-science devices.[7,8] They can also serve as building blocks for designing hierarchical materials, including aerogels[9,10] and emulsions,[11] but also nanodevices or templates with appropriate process or surface modification.[7,8]

They have thus been recently assessed as porogen building blocks for the synthesis of metal oxides which are generally obtained after thermal oxidation of this biotemplate.[12,13] This is especially true in the case of TiO_2, a widely applied material in the field of photocatalysis,[14] while also showing interesting properties as negative electrode in electrochemical devices.[15−19] Such templating or replication of cellulosic fibers is generally performed by infiltration/deposition of a metal oxide sol, e.g. for TiO_2,[20−22] but may be limited for precise replication of cellulosic nanostructures. ALD has been successfully used on NFC aerogels for this purpose, but NFC replication requires a sophisticated ALD process and high temperatures (190 °C) in the case of TiO_2,[23−25] SiO_2, and HfO_2.[26]

Following preliminary experiments with filter paper, we are now seeking ways to preserve the structure of NFC nanofibrils upon this mineralization and to form a new TiO_2@NFC nanocomposite. The chosen starting material is an aerogel obtained through freeze-drying of a solvent-exchanged suspension in order to preserve the accessibility of the cellulosic surface,[10] leading to NFC with a high specific surface area (≈100 $m^2\ g^{-1}$). The aim is to form a sheath of TiO_2 grown with-and-on cellulose nanofibrils by its chemical reaction with titanium(IV) chloride. Thus, this TiO_2@NFC is potentially the precursor of two very attractive materials, either porous metal oxide nanotubes or tubular nanocomposites of carbon (inside) and metal oxide (outside), this being only dependent on the post-thermal treatment (Figure 2). In our case, thermal oxidation of the cellulosic residue of TiO_2@NFC can lead to TiO_2 with a porous inorganic nanotube morphology (TiO_2-NT), with such material being highly a demanded solar cell,[27] photocatalyst, and negative electrode material for Li-ion batteries.[14,28−34] On the other hand, thermal conversion of the cellulosic residue into carbon upon pyrolysis can lead to TiO_2@C nanocomposites, a route rarely explored in the field of biotemplating and that we report, to the best of our knowledge, for the first time. Such TiO_2@C nanocomposites can be prepared by a reductive thermal or hydrothermal process with biochemicals such as furfural,[35,36] and they have potential applications in photocatalysis efficiency,[37] supercapacitors,[38] Li-ion batteries.[39,40]

Even though the current commercial negative electrode material in Li-based systems is graphite, which is available worldwide and features good Li insertion properties, technological progress requires faster, safer, lighter, and higher capacity battery materials. Among other interesting candidates, TiO_2 and lithium titanates show similar environmental benignancy and cost-effectiveness as graphite, but have superior safety and rate capability, providing high charge and discharge rates.[41] Their working potential of about 1.5 V vs Li^+/Li constitutes an intrinsic Li overcharge protection, impeding Li plating at high rates, while suiting the potential stability window of common organic electrolytes.[42] While the spinel $Li_4Ti_5O_{12}$ can be considered as a reference material for lithium titanates in battery applications,[43] also pure TiO_2 polymorphs such as anatase and TiO_2(B) show promising Li insertion properties.[44,45] Both polymorphs have a theoretical capacity of 336 mA h g^{-1}—corresponding to the insertion of one mole of lithium per mole of TiO_2. Such a capacity, however, is practically impossible to obtain without nanostructuring. In fact, using nanostructured TiO_2 as active lithium insertion material offers the opportunity not only to overcome the low electron and ion conductivities imposed by bulk structure but also to enhance the rate and cycling performance by increasing electrode−electrolyte contact area and surface to volume ratio.[46,47] Such open structures permit higher diffusion rates due to surface diffusion as well as easy accessibility. In this paper, we present the mineralization/replication of nanofibrils of NFC into NT-TiO_2 and TiO_2@C that were characterized and assessed in the formulation of negative electrode materials for Li-ion batteries.

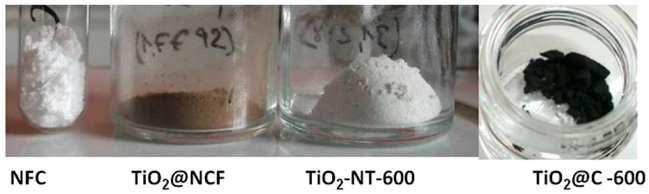

Figure 2. Picture of the materials at different preparation stages.

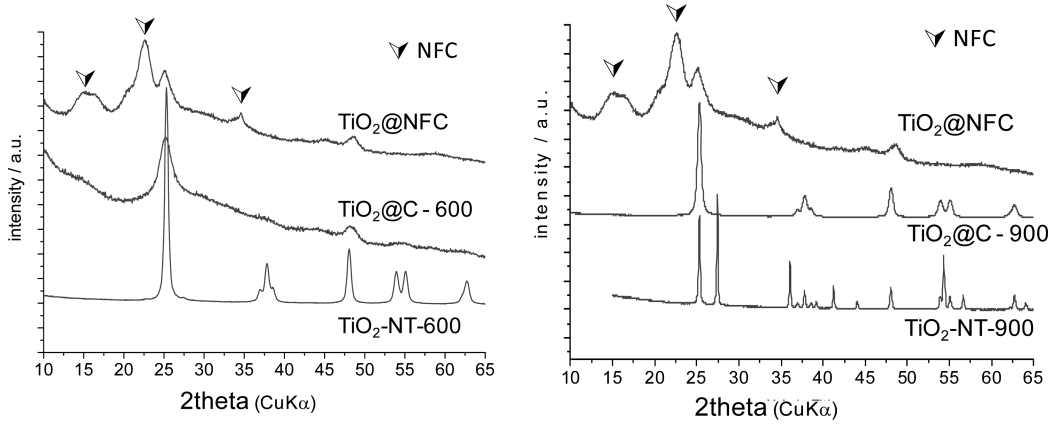

Figure 3. X-ray powder diffraction patterns of samples before and after thermal treatment in air or argon at either 600 or 900 °C.

DOI: 10.1021/acsami.5b00299
ACS Appl. Mater. Interfaces 2015, 7, 14584−14592

RESULTS AND DISCUSSION

In strictly anhydrous conditions and using dried NFC aerogels, direct mineralization of the surface of NFC nanofibrils was achieved by treatment with $TiCl_4$ at 80 °C in an autoclave under autogenous pressure. These conditions are similar to the nonhydrolytic process that inspired this work. Different reactions are assumed to occur during the treatment: Ti−Cl alcoholysis with the primary and secondary alcohol group of cellulose, and a Ti−Cl/C-O exchange as in nonhydrolytic sol−gel. The reaction of $TiCl_4$ with a residual amount of crystallization water also cannot be excluded.[48] Another possibility is the formation of water by dehydration, a process that generally occurs at temperatures above 150 °C, but that could be activated by the presence of $TiCl_4$ and acidic conditions.

Apart from the color, the TiO_2@NFC material recovered after mineralization and drying looked similar to the NFC aerogel: the centimeter scale, the shape, the mechanical consistency, and the flexibility of the initial NFC aerogel were mostly preserved. The black color of the TiO_2@NFC sample suggested at least partial carbonization of fibrils, but TiO_2 was already present as a poorly crystallized anatase phase as revealed by XRPD (crystallite size <5 nm, Figure 3 and Table S1). Unreacted cellulose is revealed by signals at 14−16°, 22.5°, and 34.5°, similar to pristine NFC.

Therefore, the cellulosic residue before any thermal treatment was apparently a mix of "chemically carbonized" and pristine cellulose. No characterization of TiO_2@NFC was possible by Raman due to extreme fluorescence phenomena.

Solid state NMR spectra obtained on TiO_2@NFC are displayed in Figure 4 and show interesting features. First, as

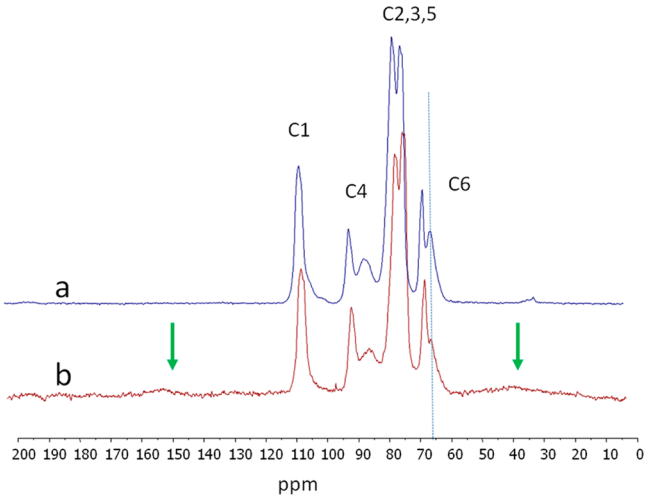

Figure 4. Solid state NMR spectra of (a) pristine nanocellulose and (b) TiO_2@NFC.

indicated by the XRPD experiments, pristine cellulose was partially preserved during the process. More interestingly, two very broad signals around 150 and 40 ppm (shown by arrows), typical of char formation,[49] indicated that part of the cellulose had been degraded. Even though the quantization could be rather delicate in the case of carbonization of cellulose, the overall contribution of degradation products could be estimated at around 10%. Cellulose preserved its crystalline structure, but even more strikingly, the decrease in the signal at 62 pmm (indicated by a dashed line) was a strong indication of a selective topochemistry of the reaction. Indeed, this signal was identified as originating from the C6 hydroxymethyl group pointing out of the cellulosic surface, with its crystalline analogs being located at 65 ppm. As already observed for surface restricted reactions on nanocellulose oxidation,[50] or esterification,[10] the relative decrease of the surface signal is a very good marker of the substitution of the surface hydroxyls. In what they have been transformed is unfortunately impossible with ^{13}C CP-MAS experiments

At the nanometer scale, prior to any thermal treatment, TiO_2@NFC appears to be homogeneous and continuous, more or less aggregated, and identical to NFC aerogel (SEM and TEM analysis (Figures 5 and S4)). However, at high magnification, the fibrils look like nano-thorns, a distinctive feature associated with the presence of elongated inorganic nanoparticles. The presence of these is likely related to the formation of TiO_2 needles and rods that we described in a previous publication.[3,4]

By thermogravimetric analysis of TiO_2@NFC in air (see Figure S1), a fast and substantial weight loss occurs above 150 °C, attributed to carbonization followed by combustion, leading to a total weight loss of 65−70% at 475−500 °C (the weight loss of pristine NFC is approximately 98% in air). Thus, upon calcination at 600 °C and 900 C, TiO_2-NT-600 and TiO_2-NT-900 are almost pure titanium dioxide, while elemental analysis reveals a carbon content of under 1% (Table 1). Accordingly, the mass ratio in the starting TiO_2@NFC could be estimated at 30−35% of TiO_2 plus 65−70% of cellulosic residue.

In argon, the weight loss is slightly delayed but continues until 1000 °C. The final weight loss at this temperature is 35−40% and should be compared to the 77% weight loss of pure NFC in the same conditions. Therefore, a hight proportion of carbon residue remains in TiO_2@C-600 and TiO_2@C-900, i.e. approximately 37% and 32%, respectively, as determined by elemental analysis (Table 1). Upon calcination in air, the weight loss of the pyrolyzed samples is approximately 49% and 42%, indicating possible underestimation of the carbon content by elemental analysis of the sample after pyrolysis at 600 and 900 °C (Table 1).

After thermal treatment, anatase is the only crystallized phase at 600 °C either under argon or air (Figure 3), while rutile is only detected after calcination at 900 °C (see Figure S3). Carbonaceous residues produced and left upon pyrolysis limit the growth of the anatase crystallite (here <20 nm, see Figure S3) and prevent the anatase-to-rutile transformation.[51]

Anatase is also identified in the calcined sample by Raman spectroscopy in all the samples (145, 196, 395, 516, 637 cm^{-1}), with rutile only being detected in TiO_2-NT-900 (437, 613 cm^{-1}) (see Figure S2). In TiO_2@C-600 and TiO_2@C-900 samples, the same analysis shows marked heterogeneity of the material resulting from the mixture of carbonaceous fibers and titania particles. Two broad signals attributed to 6-membered aromatic rings in graphitic materials are observed at 1350 and 1325 cm^{-1} related to A_{1g} (D band, attributed to defect in graphite) and at 1583−1593 cm^{-1} that are related to E_{2g} (G band, ascribed to sp^2 hybridized carbon network) (see Figure S2).[52] Due to the heterogeneity of the material, the exploitation of these signals through determination of the I_D/I_G ratio is not very significant; a correlation length of the graphitic domain in the 1−1.25 nm range seems to be present for TiO_2@C-600 and TiO_2@C-900.

In terms of morphology, the nano-thorn-like structure is preserved upon thermal treatment, i.e. either pyrolysis or

DOI: 10.1021/acsami.5b00299
ACS Appl. Mater. Interfaces 2015, 7, 14584−14592

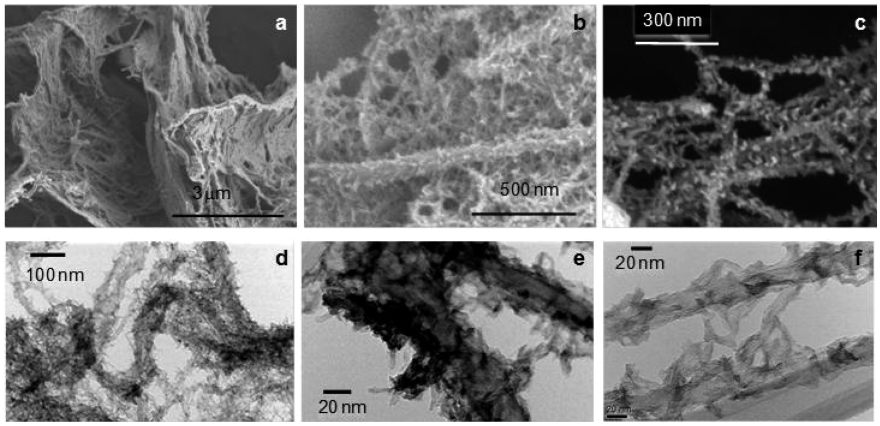

Figure 5. Images of NFC (SEM, a) and TiO_2@NFC (SEM, b–c; TEM, d–f).

Table 1. Elemental composition of the sample as determined by chemical elemental analysis and EDX

	Chem elem anal (wt %)		EDX (wt %)				
Sample	C	H	Ti	O	C	Cl	Wt loss (TGA until 1000 °C)
TiO_2@NFC	28.22	5.32	18.83	35.67	37.99	7.50	73.58%
TiO_2-NT-600	0.55	0.45	49.26	43.65	7.07	00.02	0%
TiO_2-NT-900	0.06	0.08	56.55	41.82	1.53	0.00	0%
TiO_2@C-600	37.70	1.61	28.44	28.98	41.25	1.34	49.06%
TiO_2@C-900	32.56	0.82	35.95	29.46	34.27	0.17	42.56%

calcination, at 600 or 900 °C as shown on the SEM images in Figures 6 and 7.

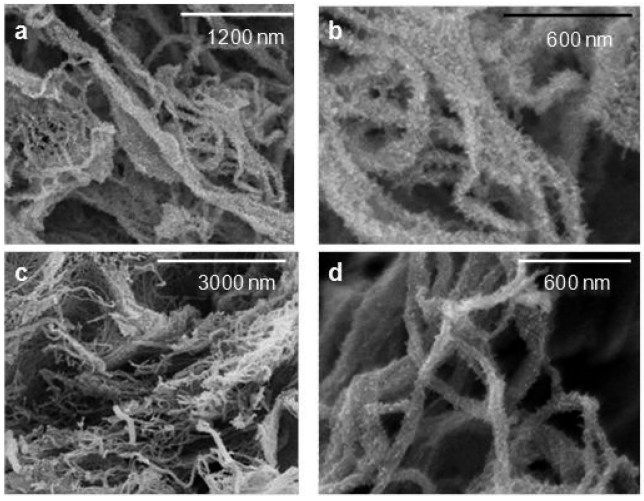

Figure 6. SEM images of TiO_2-NT-600 (a and b) and TiO_2@C-600 (c and d).

According to TEM and HRTEM analyses (Figure 7), the thorn needles are due to elongated nanoparticles of 10–20 nm associated with aggregated nanocrystals (5 < size < 30 nm) having a more or less rounded shape (Figure S4). No significant differences could be distinguished by TEM and SEM between the calcined sample and those pyrolyzed (Figure S3). However, according to the substantial weight losses observed upon calcination, we could conclude on the formation of a hollow structure in the case of TiO_2-NT-600 and TiO_2-NT-900, with a good preservation of the imprint left by the NFC.

Assessment of the texture of these materials by porosimetry measurements indicated a marked effect of the thermal treatment (in SI Table S1). Compared to pyrolysis, calcination was detrimental in terms of specific surface area and led to larger pores. As seen above, the presence of carbon during pyrolysis prevented crystal growth. However, the data collected on the sample after pyrolysis was the sum of the texture of the carbon residue and that of the oxide.

Biotemplating cellulose with titania has been known since the seminal work by Shimizu et al. using TiF_4,[53] and then the process was further developed for the formation of TiO_2 nanotubes[54] or titania/carbon composite nanocomposites[55,56] This was also the case here, but the process also allowed the formation of TiO_2 nanocrystals with an unexpected morphology. We highlighted that the situation was very different compared to previously reported biotemplating, first because no water was introduced to form the metal oxide, second because of the extremely low solubility of TiO_2 in organic solvent (CH_2Cl_2), and third because the chemical process involved the reactivity of the cellulose functionalities. The unusual morphology of the TiO_2 nanoparticles could be related to the growth process that occurs by reaction at-and-with the cellulose interface; the effect of the solvent could also play a role as demonstrated in the case of nonhydrolytic Sol–Gel.[57,58]

Lithium insertion/deinsertion properties were evaluated vs lithium metal at a C/20 current rate (where C is set at 335.6 mAh g^{-1} for a 1 e^-/h process). The galvanostatic charge–discharge profiles of the first four cycles for TiO_2 vs Li between 2.5 and 1.2 V are displayed in Figure 8a. First of all, both discharge and charge curves show a smooth slope, with the absence of a voltage plateau. Due to the contribution of the nanocellulose-derived carbon (Figure S5), a high irreversible insertion of Li is measured upon the first discharge, with a reversible charge capacity of approximately 125 mAh g^{-1}. For clarity, hereafter we only present the reversible cycling. The overall features of the galvanostatic curves are similar to the

DOI: 10.1021/acsami.5b00299
ACS Appl. Mater. Interfaces 2015, 7, 14584–14592

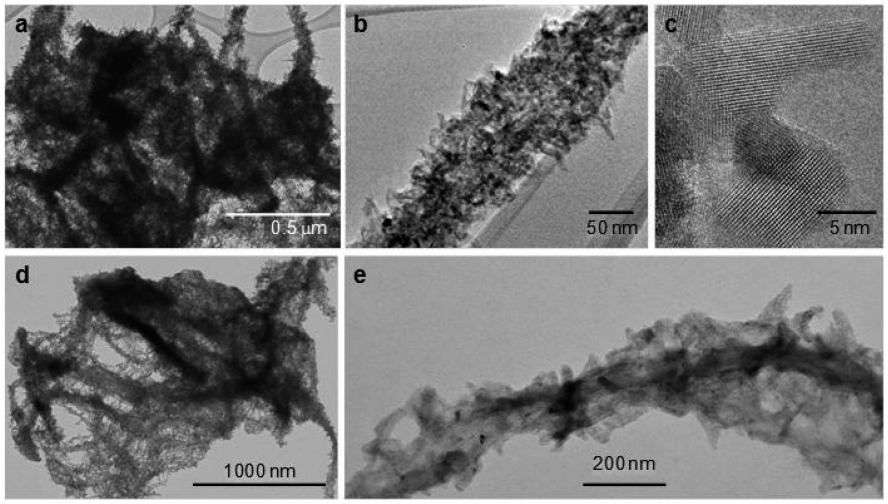

Figure 7. TEM images of TiO_2-NT-600 (a, b, and c) and TiO_2@C-600 (d and e).

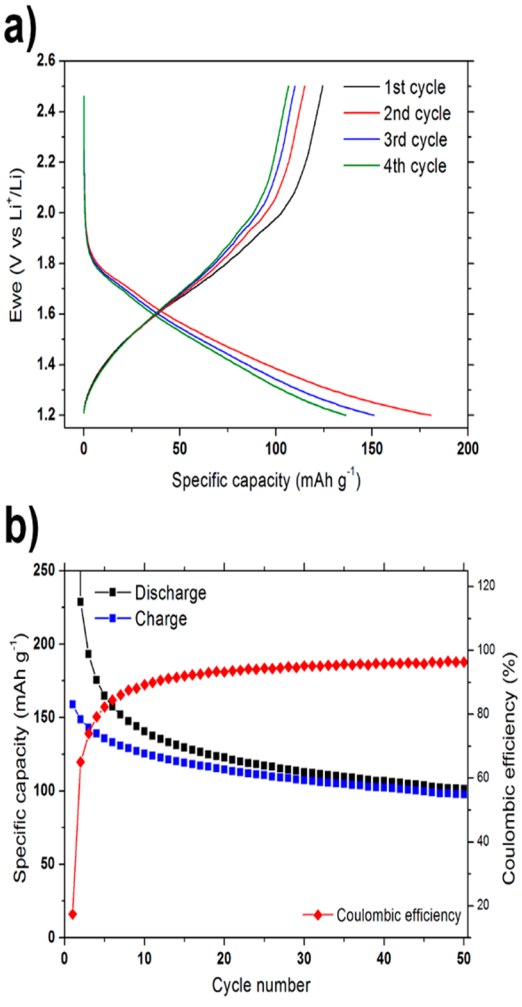

Figure 8. Galvanostatic voltage profiles for TiO_2@C-600/Li cells cycled at C/20 between 2.5 and 1.2 V versus Li^+/Li (a); charge–discharge cyclability curves of TiO_2@C-600 nanocrystals at C/20, and the corresponding Coulombic efficiency (b).

results obtained for other TiO_2 nanoparticles.[59] The constant-voltage plateau, a two-phase region where the anatase and lithium titanate phases coexist during Li^+ insertion, is usually much shorter for small particles than for larger ones, and is even absent in certain cases.[59,60] Indeed, lithium insertion into TiO_2 shows three major storage mechanisms: (i) a rapid potential drop to ca. 1.7 V vs the Li^+/Li characteristics of the formation of a solid-solution $Li_\varepsilon TiO_2$, where ε depends on particle size;[61] (ii) a two-phase reaction between the tetragonal $Li_\varepsilon TiO_2$ and the orthorhombic lithium titanate $Li_{0.5\pm\delta}TiO_2$ inducing a constant-voltage plateau around 1.7 V; followed by (iii) another two-phase reaction up to 1 V toward rock-salt-type tetragonal $LiTiO_2$.[62] The irreversibility of the latter mechanism is usually overcome through nanostructuration of the electrode material, which induces monophasic reversible pseudocapacitive interfacial storage.[60] Nevertheless, below a certain size of TiO_2 nanoparticles, the two phases at 1.7 V do not coexist and less lithium is required to give rise to the orthorhombic lithium titanate phase, hence the absence of a voltage plateau.[61] Thus, the galvanostatic results presented in Figure 8a could be understood by taking the nanoscopic nature of the TiO_2@C-600 titanium dioxide sample into account.

As displayed in Figure 8b, a TiO_2@C-600/Li half-cell can sustain a specific capacity of more than 125 mAh g^{-1} at a current density of C/20 for tens of charge–discharge cycles between 2.5 and 1.2 V, before slowly decreasing toward 100 mAh g^{-1}. Regarding the composition, the discharge capacity would correspond to the insertion of approximately 0.6 to 0.4 Li^+ ions for the first cycles, with only 0.3 Li^+ ions being reversibly inserted after 50 cycles. At the same time, the Coulombic efficiency reaches 96%, a relatively low value indicating detrimental lithium consumption during cycling. This might be due to the high surface area of TiO_2@C-600 (271.8 m^2 g^{-1}, see Table S1), or from the intrinsic carbon arising from the pyrolyzed nanocellulose (Figure S5), that would impact the electrochemical behavior by continuously inducing either electrolyte decomposition or the formation of solid–electrolyte interface (SEI) Li-based products.[63]

Cyclic voltammograms of TiO_2@C-600/Li half-cells at various scan rates from 0.25 to 5 mV s^{-1} are presented in Figure 9a. In line with the previous galvanostatic results, a very broad band is observed in the 1.2–2.5 V range on the anodic curves during cycling at various rates. The maximum current response on the anodic curves is obtained between 1.7 and 1.9 V vs Li^+/Li, a value that is in good agreement with previous studies.[16,59,64] Nonetheless it is quite difficult to visually resolve the currents on the cathodic scans. This obviously indicates an

DOI: 10.1021/acsami.5b00299
ACS Appl. Mater. Interfaces 2015, 7, 14584–14592

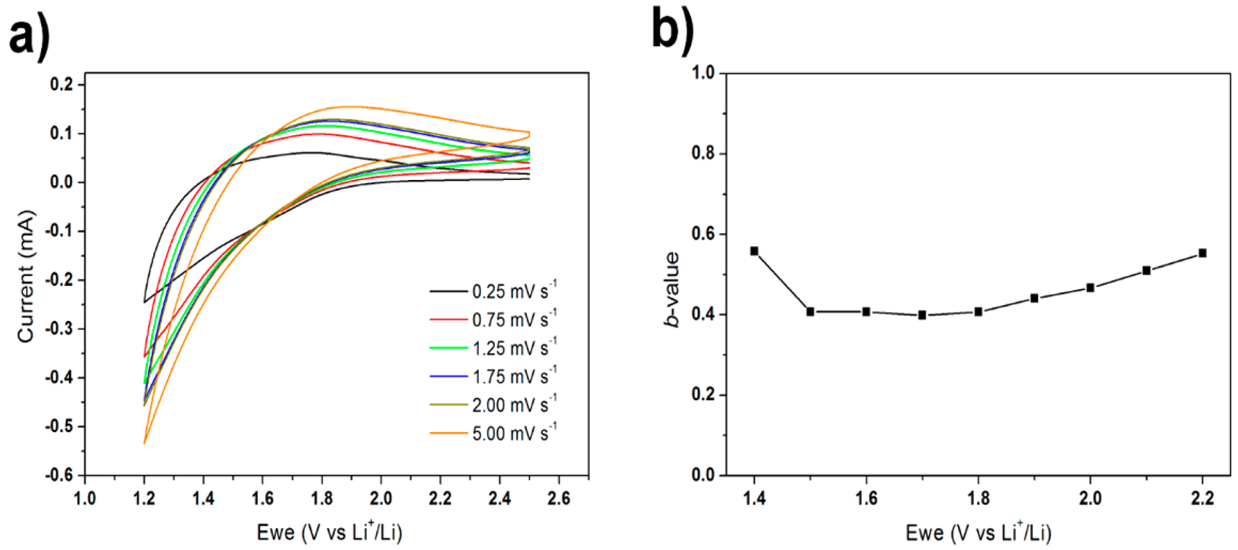

Figure 9. Cyclic voltammetry curves of TiO_2@C-600 nanocrystals at various scan rates, from 0.25 to 5.00 mV s^{-1} (a); calculated *b*-values for a TiO_2@C-600 electrode as a function of the anodic (lithium extraction) sweep (b).

emphasized pseudocapacitive behavior that could well be explained by the nanometric size of the TiO_2@C-600 material or the presence of amorphous TiO_2 mixed along with the poorly crystallized anatase phase.[6,65]

To obtain more in-depth details in the understanding of the Li-storage mechanism in nanocellulose-based TiO_2 particles, the origin of the stored charge could be unravelled through analysis of cyclic voltammetry curves. Briefly, the total stored charge can be divided into the faradaic contribution from the Li^+-insertion process, the pseudocapacitance surface effects, and the nonfaradaic contribution from the double layer effect. In order to distinguish between each contribution over the studied potential range, cyclic voltammetry data at various scan rates were analyzed according to[64]

$$i = a\nu^b$$

where the measured current i obeys a power law relationship with the scan rate ν. This method has been successfully applied to TiO_2 electrode materials versus lithium, where both a and b are adjustable parameters with *b*-values extracted from the slope of the fit of the log i vs log ν plot.[16,64] For a capacitive response, the *b*-values would approach a value of 1.0, while a faradaic contribution would induce *b*-values close to 0.5.[66] The calculated *b*-values for a TiO_2@C-600/Li half-cell are shown in Figure 9b. At the peak potentials of 1.7−1.9 V for anodic processes, the *b*-values are close to 0.5. This shows that the currents arise primarily from the Li^+ insertion into TiO_2. Nevertheless the *b*-values are close to 0.5 throughout the potential range, from 1.4 to 2.2 V for the anodic processes. Although surprising at first, this result highlighted that other faradaic contributions are to be taken into consideration. For instance, as underlined by the limited Coulombic efficiency (Figure 8b), the electrolyte decomposition would also contribute to the whole observed cell electrochemical mechanism.

CONCLUSION

This study evidences the possibility of preparing nanofibrillated TiO_2 or TiO_2@C structures by direct mineralization of NFC aerogels of high specific surface with $TiCl_4$ in anhydrous condition. Unlike ALD and Sol−Gel deposition, this nano-replication of a biotemplate lead to an unusual nano-thorn morphology for the replica. The thermal treatment applied after mineralization is a key step that allows preparation of hollow nanostructure upon calcination or nanoassemblies upon pyrolysis. Such nanomaterials have potential for different applications such as photocatalysis or electrochemical. Concerning the latter case, even though the performance in terms of the specific capacity and rate capability in this preliminary study did not turn out to be better than previous performances, this new synthesis approach—by allowing the formation of TiO_2 with an unusual morphology, tunable porosity, and TiO_2-carbon nanocomposites—will undoubtedly generate interesting surface and conductivity properties to improve the performance of as-modified TiO_2 electrodes in LiB.

EXPERIMENTAL PART

Titanium(IV) chloride ($TiCl_4$) and dichloromethane (CH_2Cl_2) were purchased from Acros (France); all the other reagents were of analytical grade. Dichloromethane was freshly distilled over P_2O_5 before use. An aerogel of nanofibrillated cellulose (NFC) was prepared by freeze-drying from *tert*-butanol solvent exchanged suspensions according to the procedure previously described;[10] it was dried for 3 days in an oven at 80 °C just before use. All manipulations with $TiCl_4$ and dried nanocellulose aerogel were performed in a glovebox under argon atmosphere (<10 ppm of water).

Instrumentation. The X-ray powder diffraction (XRPD) patterns of the samples were recorded using a diffractometer (Philips X'Pert Pro, Netherlands). Raman spectra were obtained using Horiba LabRAM ARAMIS, Japan, with excitation wavelength of 633 nm. Transmission electronic microscopy (TEM) images were recorded using JEOL 1200 EXII, JEOL, Japan, and scanning electronic microscopy (SEM) images were obtained with an Hitachi S-4800, Canada. Energy dispersive X-ray analysis (EDX) was done using the EDAX attachment (Oxford Instruments, U.K.) of the SEM system. N_2-physisorption isotherms were obtained at 77 K using Micromeritics Tristar, USA. The samples were outgassed for 12 h at 150 °C under vacuum (2 Pa). The pore size distribution was calculated from the desorption branch using the BJH method. Thermogravimetric analyses (TGA) were obtained using a Netzsch Simultaneous Thermal Analyzer STA 409 PC Luxx and Setaram Labsys TGA-DSC. All electrochemical characterizations were performed in coin cells at room temperature on an MPG2 instrument from BioLogic by using

DOI: 10.1021/acsami.5b00299
ACS Appl. Mater. Interfaces 2015, 7, 14584−14592

CR2032-type coin cells. All electrodes were composed of the active material (about 80% by weight, w/w), acetylene black (8% w/w, Y50A), and carboxymethylcellulose (12% w/w, Sigma-Aldrich). After stirring in water, the mixture was spread uniformly at 150 μm onto a copper current collector using a 3540 bird film applicator from Elecometer. Lithium metal disks were used both as reference and counter electrodes, and Whatman glass fibers filters were used as separator. The electrolyte was 1 M $LiPF_6$ in a 1:1:3 solution of ethylene carbonate, propylene carbonate, and dimethylcarbonate with 5% fluoroethylene carbonate and 1% vinylene carbonate. All electrochemical analyses were done by taking into account the mass of TiO_2. For galvanostatic measurements, the cells were cycled at C/20 between 2.5 and 1.2 V. For cyclic voltammetry, all cells were cycled at various scan rates ranging from 0.1 to 5 mV s^{-1} (0.10, 0.25, 0.50, 0.75, 1.00, 1.25, 1.50, 1.75, 2.00, 3.00, 4.00, 5.00). All calculations based on cyclic voltammetry were done by using procedures described in the literature.[16,59,64,66]

Preparation of TiO_2@NFC. In the Teflon liner of an autoclave, nanocellulose (0.60 g, 11.5 mmol assuming that NFC is 100% pure cellulose) is immersed in a solution of titanium tetrachloride (1.50 g, 4.56 mmol) in dichloromethane (30 mL). The autoclave is then kept in an oven at 85 °C for 6 days. After cooling, the resulting black popcorn-like foam is washed with dichloromethane (3 × 30 mL of anhydrous dichloromethane); the resultant solid (≈0.9 g) is labeled as TiO_2@NFC.

Preparation of calcined samples TiO_2-NT-600 and TiO_2-NT-900. Part of TiO_2@NFC was calcined at 600 °C for 1 h with a ramping rate of 5 °C min^{-1} leading to the sample TiO_2-NT-600. Part of TiO_2@NFC was calcined at 900 °C for 15 min with a ramping rate of 10 °C min^{-1} leading to the sample TiO_2-NT-900.

Preparation of pyrolysed samples TiO_2@C-600 and TiO_2@C-900. Part of TiO_2@NFC was pyrolyzed at 600 °C for 1 h with a ramping rate of 5 °C min^{-1} leading to the sample TiO_2@C-600. Part of TiO_2@NFC was pyrolyzed at 900 °C for 15 min with a ramping rate of 10 °C min^{-1} leading to the sample TiO_2@C-900.

■ ASSOCIATED CONTENT

Supporting Information

TGA analysis of TiO_2@NFC, RAMAN spectra of the samples after thermal treatment, porosimetry measurement of sample after thermal treatment (Table 1), SEM images of NFC before any treatment and of TiO2-NT 900, and HRTEM images of elongated nanocrystals of TiO_2 anatase in TiO_2-NT900. This material is available free of charge via the Internet at http://pubs.acs.org.

■ AUTHOR INFORMATION

Corresponding Author

*E-mail: bruno.boury@univ-montp2.fr.

Funding

The authors thank the Institute Charles Gerhardt, Institut Carnot Chimie Balard, Pole Balard, and Labex ChemMISyst for financial support.

Notes

The authors declare no competing financial interest.

■ ACKNOWLEDGMENTS

The authors would like to gratefully acknowledge Hyungseok Kim, Jesse Ko, Sarah Tolbert, and Bruce Dunn for their help on the *b*-values calculations. The authors gratefully acknowledge G. Clavel, who performed the HTRM analysis at Max Planck Institute in Potsdam.

■ REFERENCES

(1) Caruso, R. A.; Antonietti, M. Sol-Gel Nanocoating: An Approach to the Preparation of Structured Materials. *Chem. Mater.* **2001**, *13* (10), 3272−3282.
(2) Huang, J.; Gu, Y. Self-Assembly of Various Guest Substrates in Natural Cellulose Substances to Functional Nanostructured Materials. *Curr. Opin. Colloid Interface Sci.* **2011**, *16* (6), 470−481.
(3) Nair, G. R.; Samdarshi, S. K.; Boury, B. Surface Mineralization of Cellulose by Metal Chloride − an Original Pathway for the Synthesis of Hierarchical Urchin and Needle Carpetlike TiO_2 Superstructures. *Eur. J. Inorg. Chem.* **2013**, *30*, 5303−5310.
(4) Boury, B.; Nair, R. G.; Samdarshi, S. K.; Makiabadi, T.; Mutin, P. H. Non-hydrolytic synthesis of hierarchical TiO_2 nanostructures using natural cellulosic materials as both oxygen donors and templates. *New J. Chem.* **2012**, *36* (11), 2196−2200.
(5) Eichhorn, S. J.; Dufresne, A.; Aranguren, M.; Marcovich, N. E.; Capadona, J. R.; Rowan, S. J.; Weder, C.; Thielemans, W.; Roman, M.; Renneckar, S.; Gindl, W.; Veigel, S.; Keckes, J.; Yano, H.; Abe, K.; Nogi, M.; Nakagaito, A. N.; Mangalam, A.; Simonsen, J.; Benight, A. S. Review: Current International Research into Cellulose Nanofibres and Nanocomposites. *J. Mater. Sci.* **2010**, *45* (1), 1−33.
(6) Bi, Z.; Paranthaman, M. P.; Menchhofer, P. A.; Dehoff, R. R.; Bridges, C. A.; Chi, M.; Guo, B.; Sun, X.-G.; Dai, S. Self-Organized Amorphous TiO_2 Nanotube Arrays on Porous Ti Foam for Rechargeable Lithium and Sodium ion Batteries. *J. Power Sources* **2013**, *222*, 461−466.
(7) Klemm, D.; Kramer, F.; Moritz, S.; Lindström, T.; Ankerfors, M.; Gray, D.; Dorris, A. Nanocelluloses: A New Family of Nature-Based Materials. *Angew. Chem., Int. Ed. Engl.* **2011**, *50* (24), 5438−5466.
(8) Tingaut, P.; Zimmermann, T.; Sebe, G. Cellulose Nanocrystals and Microfibrillated Cellulose as Building Blocks for the Design of Hierarchical Functional Materials. *J. Mater. Chem.* **2012**, *22* (38), 20105−20111.
(9) Heath, L.; Thielemans, W. Cellulose Nanowhisker Aerogels. *Green Chem.* **2010**, *12* (8), 1448−1453.
(10) Fumagalli, M.; Ouhab, D.; Boisseau, S. M.; Heux, L. Versatile Gas-Phase Reactions for Surface to Bulk Esterification of Cellulose Microfibrils Aerogels. *Biomacromolecules* **2013**, *14* (9), 3246−3255.
(11) Kalashnikova, I.; Bizot, H.; Cathala, B.; Capron, I. New Pickering Emulsions Stabilized by Bacterial Cellulose Nanocrystals. *Langmuir* **2011**, *27* (12), 7471−7479.
(12) Schnepp, Z. Biopolymers as a Flexible Resource for Nanochemistry. *Angew. Chem., Int. Ed. Engl.* **2013**, *52* (4), 1096−1108.
(13) Dujardin, E.; Blaseby, M.; Mann, S. Synthesis of Mesoporous Silica by Sol-Gel Mineralisation of Cellulose Nanorod Nematic Suspensions. *J. Mater. Chem.* **2003**, *13* (4), 696−699.
(14) Froschl, T.; Hormann, U.; Kubiak, P.; Kucerova, G.; Pfanzelt, M.; Weiss, C. K.; Behm, R. J.; Husing, N.; Kaiser, U.; Landfester, K.; Wohlfahrt-Mehrens, M. High Surface Area Crystalline Titanium Dioxide: Potential and Limits in Electrochemical Energy Storage and Catalysis. *Chem. Soc. Rev.* **2012**, *41* (15), 5313−5360.
(15) Rauda, I. E.; Augustyn, V.; Dunn, B.; Tolbert, S. H. Enhancing Pseudocapacitive Charge Storage in Polymer Templated Mesoporous Materials. *Acc. Chem. Res.* **2013**, *46* (5), 1113−1124.
(16) Brezesinski, T.; Wang, J.; Polleux, J.; Dunn, B.; Tolbert, S. H. Templated Nanocrystal-Based Porous TiO_2 Films for Next-Generation Electrochemical Capacitors. *J. Am. Chem. Soc.* **2009**, *131* (5), 1802−1809.
(17) Brezesinski, T.; Wang, J.; Tolbert, S.; Dunn, B. Next Generation Pseudocapacitor Materials from Sol-Gel Derived Transition Metal Oxides. *J. Sol-Gel Sci. and Technol.* **2011**, *57* (3), 330−335.
(18) Tarascon, J. M.; Armand, M. Issues and Challenges Facing Rechargeable Lithium Batteries. *Nature* **2001**, *414* (6861), 359−367.
(19) Joo, J. B.; Zhang, Q.; Lee, I.; Dahl, M.; Zaera, F.; Yin, Y. Mesoporous Anatase Titania Hollow Nanostructures though Silica-Protected Calcination. *Adv. Funct. Mater.* **2012**, *22* (1), 166−174.
(20) Boury, B.; Plumejeau, S. Metal Oxides and Polysaccharides: an Efficient Hybrid Association for Materials Chemistry. *Green Chem.* **2015**, *17*, 72−88.

DOI: 10.1021/acsami.5b00299
ACS Appl. Mater. Interfaces 2015, 7, 14584−14592

(21) El Kadib, A.; Bousmina, M. Chitosan Bio-Based Organic–Inorganic Hybrid Aerogel Microspheres. *Chem.—Eur. J.* **2012**, *18* (27), 8264–8277.
(22) Quignard, F.; Renzo, F.; Guibal, E. From Natural Polysaccharides to Materials for Catalysis, Adsorption, and Remediation. *Top. Curr. Chem.* **2010**, *294*, 165–197.
(23) Kettunen, M.; Silvennoinen, R. J.; Houbenov, N.; Nykänen, A.; Ruokolainen, J.; Sainio, J.; Pore, V.; Kemell, M.; Ankerfors, M.; Lindström, T.; Ritala, M.; Ras, R. H. A.; Ikkala, O. Photoswitchable Superabsorbency Based on Nanocellulose Aerogels. *Adv. Funct. Mater.* **2011**, *21* (3), 510–517.
(24) Korhonen, J. T.; Hiekkataipale, P.; Malm, J.; Karppinen, M.; Ikkala, O.; Ras, R. H. A. Inorganic Hollow Nanotube Aerogels by Atomic Layer Deposition onto Native Nanocellulose Templates. *ACS Nano* **2011**, *5* (3), 1967–1974.
(25) Nelson, K.; Deng, Y. The Shape Dependence of Core–Shell and Hollow Titania Nanoparticles on Coating Thickness During Layer-by-Layer and Sol–Gel Synthesis. *Nanotechnology* **2006**, *17* (13), 3219–3225.
(26) Rauwel, E.; Clavel, G.; Willinger, M.-G.; Rauwel, P.; Pinna, N. Non-Aqueous Routes to Metal Oxide Thin Films by Atomic Layer Deposition. *Angew. Chem., Int. Ed. Engl.* **2008**, *47* (19), 3592–3595.
(27) Ghadiri, E.; Taghavinia, N.; Zakeeruddin, S. M.; Grätzel, M.; Moser, J.-E. Enhanced Electron Collection Efficiency in Dye-Sensitized Solar Cells Based on Nanostructured TiO_2 Hollow Fibers. *Nano Lett.* **2010**, *10* (5), 1632–1638.
(28) Deng, D.; Kim, M. G.; Lee, J. Y.; Cho, J. Green Energy Storage Materials: Nanostructured TiO_2 and Sn-based Anodes for Lithium-ion Batteries. *Energy Environ. Sci.* **2009**, *2* (8), 818–837.
(29) Zhu, G.-N.; Wang, Y.-G.; Xia, Y.-Y. Ti-based Compounds as Anode Materials for Li-ion Batteries. *Energy Environ. Sci.* **2012**, *5* (5), 6652–6667.
(30) Chen, J. S.; Tan, Y. L.; Li, C. M.; Cheah, Y. L.; Luan, D.; Madhavi, S.; Boey, F. Y. C.; Archer, L. A.; Lou, X. W. Constructing Hierarchical Spheres from Large Ultrathin Anatase TiO_2 Nanosheets with Nearly 100% Exposed (001) Facets for Fast Reversible Lithium Storage. *J. Am. Chem. Soc.* **2010**, *132* (17), 6124–6130.
(31) Liu, H.; Bi, Z.; Sun, X.-G.; Unocic, R. R.; Paranthaman, M. P.; Dai, S.; Brown, G. M. Mesoporous TiO_2–B Microspheres with Superior Rate Performance for Lithium Ion Batteries. *Adv. Mater.* **2011**, *23* (30), 3450–3454.
(32) Wang, Y.; Su, X.; Lu, S. Shape-Controlled Synthesis of TiO_2 Hollow Structures and their Application in Lithium Batteries. *J. Mater. Chem.* **2012**, *22* (5), 1969–1976.
(33) Berger, T.; Monllor-Satoca, D.; Jankulovska, M.; Lana-Villarreal, T.; Gómez, R. The Electrochemistry of Nanostructured Titanium Dioxide Electrodes. *ChemPhysChem* **2012**, *13* (12), 2824–2875.
(34) Kavan, L. Electrochemistry of Titanium Dioxide: some Aspects and Highlights. *Chem. Rec.* **2012**, *12* (1), 131–142.
(35) Titirici, M.-M.; Antonietti, M.; Baccile, N. Hydrothermal Carbon from Biomass: a Comparison of the Local Structure from Poly- to Monosaccharides and Pentoses/Hexoses. *Green Chem.* **2008**, *10* (11), 1204–1212.
(36) Zhao, L.; Chen, X.; Wang, X.; Zhang, Y.; Wei, W.; Sun, Y.; Antonietti, M.; Titirici, M.-M. One-Step Solvothermal Synthesis of a Carbon@TiO_2 Dyade Structure Effectively Promoting Visible-Light Photocatalysis. *Adv. Mater.* **2010**, *22* (30), 3317–3321.
(37) Leary, R.; Westwood, A. Carbonaceous Nanomaterials for the Enhancement of TiO_2 Photocatalysis. *Carbon* **2011**, *49* (3), 741–772.
(38) Zhi, M.; Xiang, C.; Li, J.; Li, M.; Wu, N. Nanostructured Carbon-Metal Oxide Composite Electrodes for Supercapacitors: a Review. *Nanoscale* **2013**, *5* (1), 72–88.
(39) Centi, G.; Perathoner, S. The Role of Nanostructure in Improving the Performance of Electrodes for Energy Storage and Conversion. *Eur. J. Inorg. Chem.* **2009**, *2009* (26), 3851–3878.
(40) Ming, J.; Wu, Y.; Nagarajan, S.; Lee, D.-J.; Sun, Y.-K.; Zhao, F. Fine control of Titania Deposition to Prepare C@TiO_2 Composites and TiO_2 Hollow Particles for Photocatalysis and Lithium-ion Battery Applications. *J. Mater. Chem.* **2012**, *22* (41), 22135–22141.
(41) Dylla, A. G.; Henkelman, G.; Stevenson, K. J. Lithium Insertion in Nanostructured TiO_2(B) Architectures. *Acc. Chem. Res.* **2013**, *46*, 1104–1112.
(42) Brutti, S.; Gentili, V.; Reale, P.; Carbone, L.; Panero, S. Mitigation of the Irreversible Capacity and Electrolyte Decomposition in a $LiNi_{0.5}Mn_{1.5}O_4$/nano-TiO_2 Li-ion Battery. *J. Power Sources* **2011**, *196* (22), 9792–9799.
(43) Panero, S.; Reale, P.; Ronci, F.; Rossi Albertini, V.; Scrosati, B. Structural and Electrochemical Study on $Li(Li_{1/3}Ti_{5/3})O_4$ Anode Material for Lithium Ion Batteries. *Ionics* **2000**, *6* (5–6), 461–465.
(44) Zachau-Christiansen, B.; West, K.; Jacobsen, T.; Atlung, S. Lithium Insertion in Different TiO_2 Modifications. *Solid State Ionics* **1988**, *28–30*, 1176–1182.
(45) Armstrong, A. R.; Armstrong, G.; Canales, J.; García, R.; Bruce, P. G. Lithium-Ion Intercalation into TiO_2-B Nanowires. *Adv. Mater.* **2005**, *17* (7), 862–865.
(46) Guo, Y.-G.; Hu, Y.-S.; Sigle, W.; Maier, J. Superior Electrode Performance of Nanostructured Mesoporous TiO_2 (Anatase) through Efficient Hierarchical Mixed Conducting Networks†. *Adv. Mater.* **2007**, *19* (16), 2087–2091.
(47) Zhong, L.-S.; Hu, J.-S.; Wan, L.-J.; Song, W.-G. Facile Synthesis of Nanoporous Anatase Spheres and their Environmental Applications. *Chem. Commun.* **2008**, *44*, 1184–1186.
(48) Scheirs, J.; Camino, G.; Tumiatti, W. Overview of Water Evolution During the Thermal Degradation of Cellulose. *Eur. Polym. J.* **2001**, *37* (5), 933–942.
(49) Baccile, N.; Falco, C.; Titirici, M.-M. Characterization of Biomass and its Derived Char using 13C-Solid State Nuclear Magnetic Resonance. *Green Chem.* **2014**, *16* (12), 4839–4869.
(50) Montanari, S.; Roumani, M.; Heux, L.; Vignon, M. R. Topochemistry of Carboxylated Cellulose Nanocrystals Resulting from TEMPO-Mediated Oxidation. *Macromolecules* **2005**, *38* (5), 1665–1671.
(51) Shanmugam, S.; Gabashvili, A.; Jacob, D. S.; Yu, J. C.; Gedanken, A. Synthesis and Characterization of TiO_2@C Core-Shell Composite Nanoparticles and Evaluation of Their Photocatalytic Activities. *Chem. Mater.* **2006**, *18* (9), 2275–2282.
(52) Ferrari, A. C.; Robertson, J. Interpretation of Raman Spectra of Disordered and Amorphous Carbon. *Phys. Rev. B: Solid State* **2000**, *61* (20), 14095–14107.
(53) Shimizu, K.; Imai, H.; Hirashima, H.; Tsukuma, K. Low-Temperature Synthesis of Anatase Thin Films on Glass and Organic Substrates by Direct Deposition from Aqueous Solutions. *Thin Solid Films* **1999**, *351* (1–2), 220–224.
(54) Huang, J.; Kunitake, T. Nano-Precision Replication of Natural Cellulosic Substances by Metal Oxides. *J. Am. Chem. Soc.* **2003**, *125* (39), 11834–11835.
(55) Liu, X.; Gu, Y.; Huang, J. Hierarchical, Titania-Coated, Carbon Nanofibrous Material Derived from a Natural Cellulosic Substance. *Chem.—Eur. J.* **2010**, *16* (26), 7730–7740.
(56) Li, S.; Huang, J. A Nanofibrous Silver-Nanoparticle/Titania/Carbon Composite as an Anode Material for Lithium Ion Batteries. *J. Mater. Chem. A* **2015**, *3* (8), 4354–4360.
(57) Niederberger, M. Nonaqueous Sol–Gel Routes to Metal Oxide Nanoparticles. *Acc. Chem. Res.* **2007**, *40*, 793.
(58) Mutin, P. H.; Vioux, A. Nonhydrolytic Processing of Oxide-Based Materials: Simple Routes to Control Homogeneity, Morphology, and Nanostructure. *Chem. Mater.* **2009**, *21*, 582.
(59) Wang, J.; Polleux, J.; Lin, J.; Dunn, B. Pseudocapacitive Contributions to Electrochemical Energy Storage in TiO_2 (Anatase) Nanoparticles. *J. Phys. Chem. C* **2007**, *111*, 14925–14931.
(60) Shin, J. Y.; Samuelis, D.; Maier, J. Sustained Lithium-Storage Performance of Hierarchical, Nanoporous Anatase TiO_2 at High Rates: Emphasis on Interfacial Storage Phenomena. *Adv. Funct. Mater.* **2011**, *21* (18), 3464–3472.
(61) Wagemaker, M.; Borghols, W. J.; van Eck, E. R.; Kentgens, A. P.; Kearley, G. J.; Mulder, F. M. The Influence of Size on Phase Morphology and Li-ion Mobility in Nanosized Lithiated Anatase TiO_2. *Chem.—Eur. J.* **2007**, *13* (7), 2023–8.

DOI: 10.1021/acsami.5b00299
ACS Appl. Mater. Interfaces 2015, 7, 14584–14592

(62) Lafont, U.; Carta, D.; Mountjoy, G.; Chadwick, A. V.; Kelder, E. M. In Situ Structural Changes upon Electrochemical Lithium Insertion in Nanosized Anatase TiO_2. *J. Phys. Chem. C* **2010**, *114*, 1372.
(63) Liu, M.; He, Y.-B.; Lv, W.; Zhang, C.; Du, H.; Li, B.; Yang, Q.-H.; Kang, F. High catalytic activity of anatase titanium dioxide for decomposition of electrolyte solution in lithium ion battery. *J. Power Sources* **2014**, *268* (0), 882−886.
(64) Lindström, H.; Södergren, S.; Solbrand, A.; Rensmo, H.; Hjelm, J.; Hagfeldt, A.; Lindquist, S.-E. Li+ Ion Insertion in TiO_2 (Anatase). 2. Voltammetry on Nanoporous Films. *J. Phys. Chem. B* **1997**, *101* (39), 7717−7722.
(65) Guan, D.; Cai, C.; Wang, Y. Amorphous and Crystalline TiO_2 Nanotube Arrays for Enhanced Li-ion Intercalation Properties. *J. Nanosci. Nanotechnol.* **2011**, *11* (4), 3641−50.
(66) Bard, A. J.; Faulkner, L. R. *Electrochemical Method: Fundamentals and Applications*; John Wiley & Sons: New York, 1980.

DOI: 10.1021/acsami.5b00299
ACS Appl. Mater. Interfaces 2015, 7, 14584−14592